 CMES, vol.47, no.2, pp.191-216, 2009

Solution of Phase Change Problems by Collocation with Local Pressure Correction

G. Kosec[1] **and B. Šarler**[2]

Abstract: This paper explores an application of a novel mesh-free Local Radial Basis Function Collocation Method (LRBFCM) [Šarler and Vertnik (2006)] in solution of coupled heat transfer and fluid flow problems with solid-liquid phase change. The melting/freezing of a pure substance is solved in primitive variables on a fixed grid with convection suppression, proportional to the amount of the solid fraction. The involved temperature, velocity and pressure fields are represented on overlapping sub-domains through collocation by using multiquadrics Radial Basis Functions (RBF). The involved first and second derivatives of the fields are calculated from the respective derivatives of the RBF's. The energy and momentum equations are solved through explicit time stepping. The pressure-velocity coupling is calculated iteratively, with pressure correction, predicted from the local continuity equation violation [Kosec and Šarler (2008a)]. The solution procedure is assessed on the classical rectangular 2D cavity melting benchmark test [Gobin and Le Quéré (2000)] which encompasses a low Prandtl 0.02 and Stefan number 0.01 situation (metal) with Rayleigh numbers 2.51e4 and 2.5e5, and a high Prandtl 50 and Stefan number 0.1 situation (paraffin wax) with Rayleigh numbers 10e7 and 10e8. The results of the mesh free simulation of the related four cases have been compared with the results of a spectra of different numerical methods [Bertrand, Binet, Combeau, Couturier, Delannoy, Gobin, Lacroix, Quéré, Médale, Mencinger, Sadat and Vieira (1998)] in terms of liquid-solid interphase position at a fixed time, and time evolution of the average hot side Nusselt number and average cavity liquid fraction. The results show good agreement with other approaches in terms of the dynamics of the interphase boundary and complicated flow structure, despite the simplest LRBFCM implementation. The advantages of the method are simplicity, accuracy, and straightforward applicability in non-uniform node arrangements.

[1] Laboratory for Multiphase Processes, University of Nova Gorica, Slovenia, E-mail: gregor.kosec@p-ng.si

[2] Laboratory for Multiphase Processes, University of Nova Gorica, Slovenia, E-mail: bozidar.sarler@p-ng.si

Keywords: Newtonian fluid flow, Stefan problem, Gobin Le Quéré benchmark, primitive variables, natural convection, melting, local pressure-velocity coupling, mesh-free method, local radial basis function collocation method.

1 Introduction

The computational modeling of systems with solid and liquid phase has become a highly popular research subject due to its pronounced influence in better understanding of nature as well as in the development of the advanced technologies. Melting of the polar ice caps and manufacturing of nano-materials are two typical contemporary examples. The related historical, physical and computational aspects are described in monographs [Alexiades and Solomon (1993), Crank (1999), Dantzig and Rappaz (2009)] and review articles [Yao and Prusa (1989), Fukusako and Yamada (1993), Šarler (1995), Prescott and Incropera (1996), Rettenmayr (2009)]. The classical numerical methods such as the Finite Volume Method (FVM) or the Finite Element Method (FEM) are used for solving these problems in the majority of the simulations [Dantzig (1989), Viswanath and Jaluria (1993)]. Despite the powerful features of these methods, there are often substantial difficulties in applying them to realistic, geometrically complex three-dimensional transient problems. A common drawback of the mentioned methods is the need to create a polygonisation, either in the domain and/or on its boundary. This type of meshing is often the most time consuming part of the solution process and is far from being fully automated. The numerical simulations of engineering solid liquid systems are mainly based on the averaged or mixture equations, defined on the entire solid and liquid domain, with the interphase conditions, incorporated into the non-linearity of the governing equations. The proper numerical solution of these equations requires adaptation of the discretization in the vicinity of the moving boundary. The principal bottleneck in these types of numerical methods is the time consuming re-meshing of the evolving interphase boundaries and phase domains. The polygonisation problem is thus even more pronounced. The application of the alternative numerical methods to FVM and FEM, such as the mesh reduction [Šarler and Kuhn (1998b), Šarler and Kuhn (1998a), Šarler and Kuhn (1999)] or meshless [Šarler (2002)] methods, for phase change problems is relatively rare at the present.

In order to understand and numerically model the complicated phenomena that accompany dissolution/solidification of complex engineering alloys, a much simpler sub-system of melting/freezing of a pure substance, driven by natural convection, has to be studied first. Analytical solutions for melting of the pure substances in the 1D domain (Stefan's problem), where the fluid flow can be induced only by the density change due to phase change are quite well known [Šarler (1995)]. Inclusion

of the natural convection and therefore the complex flow structures in 2D makes the "simple" melting/freezing problem not amenable to closed form solution. The numerical simulation is required to obtain the behavior of such systems. Due to the complexity of the problem, neither a commonly agreed quantitative experimental data nor the commonly agreed numerical benchmark solutions are known at the present, despite the many attempts: [Jany and Bejan (1987), Viskanta (1988), Bertrand, Binet, Combeau, Couturier, Delannoy, Gobin, Lacroix, Quéré, Médale, Mencinger, Sadat and Vieira (1998), Le Quéré and Gobin (1999), Stella and Giangi (2000), Mencinger (2003), Hannoun, Alexiades and Zee Mai (2003)]. The spectrum of differing experimental data and differing simulations for the same melting systems (usually melting of tin or gallium) is enormous. It was recently even not known if the correct flow structure in certain melting systems is monocellular or multicellular [Hannoun, Alexiades and Zee Mai (2003)].

The focus in this work is to demonstrate the applicability of the recently developed mesh-free LRBFCM in melting/freezing problems and the enlargement of the spectrum of simulations of such phase change problems in the range of parameters, previously not yet published. The solution is in mesh-free methods represented on the arbitrarily distributed set of nodes without any additional topological relations between them. These mesh-free methods represent a promising technique to avoid the polygonisation problems [Kansa (1990a), Kansa (1990b), Chen (2002), Atluri and Shen (2002b), Atluri and Shen (2002a), Liu (2003), Atluri (2004), Liu and Gu (2005)]. This paper is focused on one of the simplest class of mesh-free methods in development today, the Radial Basis Function [Buhmann (2000)] Collocation Methods (RBFCM) [Šarler (2007)].

The method has been applied in different scientific and engineering problems from heat transport [Zerroukat, Power and Chen (1998)] and convective diffusive problems [Šarler, Perko and Chen (2004)] to the fluid flow problems [Šarler, Perko, Chen and Kuhn (2001)], phase change phenomena [Kovačević, Poredoš and Šarler (2003)], wave equations [Haq, ul-Islam and Arshed (2008)] and solid mechanics problems [Mai-Duy, Khennane and Tran-Cong (2007), Le, Mai-Duy, Tran-Cong and Baker (2008)], as well. The method has been formulated by integrating the partial derivatives [Mai-Duy and Tran-Cong (2003)] and applied to transient problems [Mai-Cao and Tran-Cong (2005)], fluid flow [Mai-Duy, Mai-Cao and Tran-Cong (2007)] and moving boundaries [Mai-Cao and Tran-Cong (2008)]. Different improvements have been applied such as the advanced Neumann boundary conditions treatment [Libre, Emdadi, Kansa, Rahimian and Shekarchi (2008)].

The main drawback of this global method lies in the need for solving the global matrices in order to solve the problem. The condition number of the global matrix is highly sensitive to the shape of the basis functions and the nodes distribution. The

problem becomes important even with small number of nodes ($\approx$1000). The mitigation of the related problem has been attempted by domain decomposition [Mai-Duy and Tran-Cong (2002)], multi-grid approach and compactly supported RBFs [Chen, Ganesh, Golberg and Cheng (2002)] which all represent a substantial complication of the original simple method. The radial basis functions have been first put into context of porous media flow by [Šarler, Gobin, Goyeau, Perko and Power (2000)] where the natural convection problem in Darcy porous media, and later Darcy-Brinkman porous media [Šarler, Perko, Gobin, Goyeau and Power (2004)] have been solved by the dual reciprocity boundary element method (DRBEM). This method belongs to the semi-mesh-free methods, because the domain fields are approximated by the global interpolation with the RBFs and the boundary fields by the boundary elements (polygons). The truly mesh-free RBFCM has been for the first time used for solution of Darcy porous media in [Šarler, Perko and Chen (2004)]. A substantial breakthrough in the development of the RBFCM was its local formulation, LRBFCM. Lee at al. [Lee, Liu and Fan (2003)] demonstrated that the local formulation does not substantially degrade the accuracy with respect to the global one. On the other hand, it is much less sensitive to the choice of the RBF shape. The local RBFCM has been previously developed for diffusion problems [Šarler and Vertnik (2006)], convection-diffusion solid-liquid phase change problems [Vertnik and Šarler (2006)] and subsequently successfully applied in industrial process of direct chill casting [Vertnik, Založnik and Šarler (2006)]. The algorithm was tested on the classical De Vahl Davis natural convection problem [Kosec and Šarler (2008a)] and the natural convection problem [Kosec and Šarler (2008b)] in Darcy porous media. The engineering k-epsilon turbulence modeling was implemented by [Vertnik and Šarler (2009)]. The LRBFCM represents a local variant of the already developed global RBFCM (or Kansa method) for thermo-fluid problems [Šarler, Perko, Chen and Kuhn (2001), Šarler (2005)]. An improvement of the method by adding the characteristics of he solution has been proposed [Stevens, Power, Lees and Morvan (2009)].

The present paper extends the spectra of physical problems, solved by LRBFCM, to thermo-fluid problems with phase change. The paper is structured in the following way: The governing set of mass, energy and momentum equations are given first. Special attention is focused on the description of the phase-change of pure substance. The solution procedure is described in time-discretised setting, followed by the details of the LRBFCM and numerical implementation. The performance of the developed algorithm is assessed on the melting of low Prandtl number material (tin), illustrating melting of metals, and high Prandtl number material (paraffin), illustrating the melting of organic materials. The simulated observation time of melting process is longer than previously published attempts. Due to the lack of

a reliable fine-grid reference benchmark solution for melting, additional tests are first done on a more simple system. This involves natural convection in a tall cavity with width/height aspect ratio 1/4 filled with low Pr number fluid (situation, typical for the early stage of melting of metals). The obtained LRBFCM multicellular flow results of the tall cavity case are compared with the already known reliable (discretization independent) FVM and FEM solutions, and the obtained LRBFCM results of the melting cases are compared with the spectra of the results of the Gobin and Le Quéré benchmark. The assessment of the results is followed by the conclusions and further research directions.

2 Governing equations

Consider a connected fixed domain Ω with boundary Γ occupied with the solid-liquid phase change material. The material is considered pure, i.e. phase-change occurs at a fixed sharp melting/freezing temperature T_m. All material properties are considered to be constant and equal in both phases. The main goal of this paper is the calculation of the transient temperature, velocity and pressure fields in the system by the LRBFCM. These fields are governed by the coupled mass, momentum and energy equations [Voller, Mouchmnov and Cross (2002)]. The energy transport is described through equation

$$\frac{\partial H}{\partial t} + \nabla \cdot (H\mathbf{v}) = \nabla \cdot (\lambda \nabla T) \tag{1}$$

where λ, H, T and $\mathbf{v}$ stand for time, density, thermal conductivity, enthalpy, temperature and velocity, respectively. The heat flux due to phase change is embedded into the definition of the enthalpy. The enthalpy dependence on the liquid fraction and the temperature is constituted as

$$H(T) = c_p T + f_l L \tag{2}$$

where c_p, f_l and L stand for specific heat, liquid fraction and latent heat, respectively. The enthalpy thus has a jump L at the melting/freezing temperature, i.e.

$$f_l(T) = \begin{cases} T \geq T_m; & 1 \\ T < T_m; & 0 \end{cases} \tag{3}$$

A narrow melting/freezing interval is artificially introduced instead of (3) in order to avoid the numerical instabilities. The liquid fraction is therefore constituted as

$$f_l(T) = \begin{cases} T \geq T_m + T_L; & 1 \\ T < T_m; & 0 \\ T_m + T_L > T \geq T_m; & T - T_m/T_L \end{cases} \tag{4}$$

with T_m standing for melting/freezing interval. The equation (4) collapses to the equation (3) in case $T_L = 0$.The results obtained with such phase-change intervalsmoothing are physically reasonable as long as theinterval is small enough [Dalhuijsen and Segal (1986)]. The fluid flow is described by Navier-Stokes equationsfor mass and momentum conservation.

$$\nabla \cdot \mathbf{v} = 0 \tag{5}$$

$$\frac{\partial(\rho \mathbf{v})}{\partial t} + \nabla \cdot (\rho \mathbf{v}\mathbf{v}) = -\nabla P + \nabla \cdot (\mu \nabla \mathbf{v}) + \mathbf{F} \tag{6}$$

with P, μ, ρ and $\mathbf{F}$ standing for pressure, viscosity, and body force due to gravitational acceleration, respectively. The standard Boussinesq approximation is adopted in order to model the body force

$$\mathbf{F} = \rho \left[1 - \beta_B (T - T_{\text{ref}})\right] \mathbf{g} \tag{7}$$

with $\mathbf{g}$, β_B and T_{ref} standing for gravitational acceleration, coefficient of thermal expansion and reference temperature for density. The artificially introduced phase-change interval T_L transforms the sharp phase change interphase boundary into an artificial mushy region. This region is from the fluid flow perspective usually modeled as porous media with the addition of Darcy or/and Brinkman and/or Forcheimer terms. We do not expect extensive mushy region in our case, since T_L is small. Therefore, the mushy region "porous media" is constituted in a most simple manner by suppressing the velocity field in the mushy region. This is achieved by multiplying it with the liquid fraction. This ensures proper limiting physical behaviour of velocity field (0 in the solid phase and $\mathbf{v}$ in the liquid phase).

We seek the solution of the governing equations at time $t = t_0 + \Delta t$, where t_0 represents initial time and Δt positive time increment, by assuming known initial temperature, pressure and velocity fields at time $t = t_0$: $T = T_0$; $P = P_0$; $\mathbf{v} = \mathbf{v}_0$, and known Dirichlet and Neumann boundary conditions for temperature

$$T = T_\Gamma^D; \quad \mathbf{p} \in \Gamma^D,\ t > t_0 \tag{8}$$

$$\partial T / \partial n_\Gamma = T_\Gamma^N; \quad \mathbf{p} \in \Gamma^N,\ t > t_0 \tag{9}$$

at the Dirichlet and Neumann parts of the boundary $\Gamma \cup \Gamma^D + \Gamma^N$ and the no-slip and no-penetration Dirichlet boundary conditions for velocity

$$\mathbf{v} = \mathbf{v}^D = \mathbf{0}, \quad \mathbf{p} \in \Gamma,\ t \geq t_0 \tag{10}$$

where $\mathbf{p} = \mathbf{i} p_x + \mathbf{j} p_y$ stands for position vector with Cartesian base vectors $\mathbf{i}$ and $\mathbf{j}$, and Cartesian spatial coordinates p_x and p_y.

3 Solution procedure

The solution procedure is represented in three entities. In the first one, the manipulations of the time-discretized governing equations are made. In the second one, the meshless space discretization is discussed. In the last one, the numerical implementation issues are elaborated.

3.1 Time discretization

The explicit time discretization is adopted to cope with the transience terms in momentum and energy equations. The Navier-Stokes equations (5) and (6) are solved iteratively by completely local pressure-velocity coupling, based on the pressure correction, predicted from velocity divergence (mass conservation violation).

In the *first step* the velocity is estimated from the discretized form of equation (6)

$$\hat{\mathbf{v}} = \mathbf{v}_0 + \frac{\Delta t}{\rho}\left[-\nabla P_0 + \nabla\cdot(\mu\nabla\mathbf{v}_0) + \mathbf{F}_0 - \nabla\cdot(\rho\mathbf{v}_0\mathbf{v}_0)\right] \tag{11}$$

where $\hat{\mathbf{v}}$ denotes velocity at time $t_0+\Delta t$, $\mathbf{v}_0$, P_0 denote velocity and pressure at time t_0 and Δt stands for the time-step length. The calculated velocity $\hat{\mathbf{v}}$ does not satisfy the mass continuity equation (5) in general. In order to couple mass continuity equation with the momentum equation, an iteration process is used where in the first iteration ($m=1$) the velocity and the pressure are set to

$$\mathbf{v}^m = \hat{\mathbf{v}} \tag{12}$$

$$P^m = P_0 \tag{13}$$

where m stands for iteration index. To project the velocity into the divergence free space, a velocity correction $\hat{v}$ is added

$$\nabla\cdot(\mathbf{v}^m + \hat{v}) = 0 \quad \rightarrow \quad \nabla\cdot\mathbf{v}^m = -\nabla\cdot\hat{v} \tag{14}$$

The velocity correction is assumed to be affected by the pressure correction only

$$\hat{v} = -\frac{\Delta t}{\rho}\nabla\hat{P} \tag{15}$$

where $\hat{P}$ stands for the pressure correction. The pressure correction Poisson equation is constructed by applying the divergence over equation (15)

$$\nabla^2\hat{P} = \frac{\rho}{\Delta t}\nabla\cdot\mathbf{v}^m \tag{16}$$

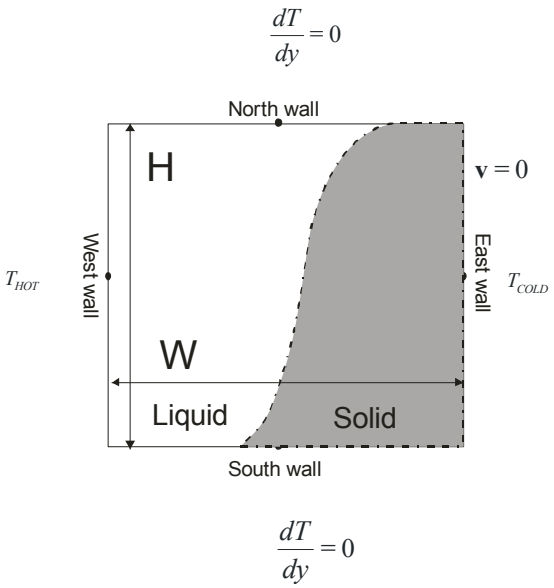

Figure 1: The considered physical system schematics

Instead of solving the equation (16) globally [Divo and Kassab (2007)] with the appropriate pressure correction boundary conditions, the pressure correction is assumed to be proportional to the Laplace of pressure correction. In the *second step*, the pressure correction is therefore calculated as

$$\hat{P} \approx \ell^2 \nabla^2 \hat{P} = \ell^2 \frac{\rho}{\Delta t} \nabla \cdot \mathbf{v}^m \tag{17}$$

where ℓ stands for the characteristic length. The assumption (17) enables [Kosec and Šarler (2008a)] for solving the problem completely locally. In the *third step*, the intermediate pressure and velocity are corrected as

$$P^{m+1} = P^m + \beta \hat{P} \tag{18}$$

$$\mathbf{v}^{m+1} = \mathbf{v}^m - \beta \frac{\Delta t}{\rho} \nabla \hat{P} \tag{19}$$

where β stands for a suitable relaxation parameter. If the criteria

$$\nabla \cdot \mathbf{v}^{m+1} < \varepsilon_v \tag{20}$$

is not met, than the iteration returns back to the equation (12), else the pressure-velocity iteration is completed and the calculation proceeds to the next step.

The energy equation (1) is solved in the *fourth step*

$$H(T) = H(T_0) + \Delta t \left[\nabla \cdot (\lambda \nabla T_0) - \nabla \cdot (H(T_0)\mathbf{v}_0)\right] \tag{21}$$

where T_0 and T denote temperature at time t_0 and $t_0 + \Delta t$. In the *fifth step*, the liquid fraction is updated by equation (2). After solution of the new enthalpy field, the temperature and the liquid fraction are updated

$$T = T(H) \tag{22}$$

$$f_l = f_l(T) \tag{23}$$

Before attempting the next time step, the velocity field is in the *sixth step* multiplied with the liquid fraction in order to disengage the convection in the solid phase

$$\mathbf{v} = f_l \mathbf{v} \tag{24}$$

3.2 Meshless spatial discretization

The pressure, velocity and temperature fields are interpolated on the coincident grid points by RBFs [Buhmann (2000)]. The calculation domain is divided into overlapping sub-domains (Figure 2). An arbitrary scalar function θ is represented on each of the local sub-domains as

$$\theta(\mathbf{p}) \approx \sum_{n=1}^{N} \alpha_n R_n(\mathbf{p}) \tag{25}$$

with $\mathbf{p}$, R_n, α_n and N standing for the RBF, the collocation coefficient and the number of the collocation points, respectively. Hardy's multiquadrics RBF's are defined as

$$R_n(\mathbf{p}) = \sqrt{r_n^2(\mathbf{p}) + c^2 r_0^2}; \quad r_n^2 = (\mathbf{p} - \mathbf{p}_n) \cdot (\mathbf{p} - \mathbf{p}_n) \tag{26}$$

where c represents a dimensionless shape parameter. The scaling parameter r_0^2 is set to the maximum nodal distance of the sub-domain. The coefficients α_n are obtained from the collocation condition which implies the exact satisfaction of the equation (25) in the nodal points. In case the number of the nodes is the same as the number of the terms in the expansion (25), the system simplifies to

$$\theta(\mathbf{p}_i) = \theta_i = \sum_{n=1}^{N} \alpha_n R_n(\mathbf{p}_i) \tag{27}$$

$$\mathbf{R}\boldsymbol{\alpha} = \boldsymbol{\theta} \tag{28}$$

where the matrix elements $R_{ni} = R_n(\mathbf{p}_i)$. Solution of the linear system of equations (28) provides the collocation coefficients α_n and therefore the spatial derivatives of the function θ can easily be obtained through derivation of the equation (25)

$$\frac{\partial}{\partial p_\sigma}\theta(\mathbf{p}) \approx \sum_{n=1}^{N} \alpha_n \frac{\partial}{\partial p_\sigma} R_n(\mathbf{p}) \tag{29}$$

$$\frac{\partial^2}{\partial^2 p_\sigma}\theta(\mathbf{p}) \approx \sum_{n=1}^{N} \alpha_n \frac{\partial^2}{\partial^2 p_\sigma} R_n(\mathbf{p}) \tag{30}$$

where $p_{\sigma=x,y}$. All necessary derivatives to construct the involved divergence, gradient and Laplace operators can be calculated through equations (29) and (30). All matrix elements R_{ni} need to be evaluated only once before time-stepping begins.

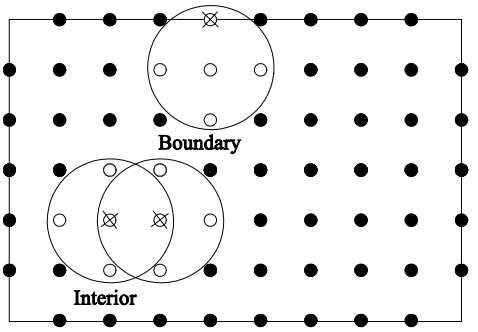

Figure 2: The discretization schematics

Only the simplest sub-domains with five equidistant points are used in the present paper. The described collocation method and five nodded sub-domains are schematically represented in Figure 2. Such five nodded collocation sub-domains are used to approximate the first and the second spatial derivatives in the central sub-domain nodes. The derivative instead of the function value is prescribed at the boundary collocation points with the Neumann boundary conditions. The Equation (27) is in such Neumann points $\mathbf{p}_i$ replaced by

$$\frac{\partial}{\partial p_\sigma}\theta(\mathbf{p}_i) = \sum_{n=1}^{N} \alpha_n \frac{\partial}{\partial p_\sigma} R_n(\mathbf{p}_i) \tag{31}$$

3.3 Numerical implementation

The represented algorithm is completely explicit and local, including also the pressure velocity coupling, and therefore it can be straightforward efficiently parallelized. All routines have been written in the C++ language with LAPACK based

IMKL numerical library included. The parallelization is implemented with OpenMP protocol.

4 Numerical examples

Two physically different test case families are computed and discussed in order to assess the behavior of the method. First, the natural convection in a tall cavity and second, melting driven by natural convection. In both cases, a rectangular cavity is considered. The left and the right walls are set to different temperatures while the top and the bottom walls are insulated in both cases. All walls are solid and impermeable.

All numerical examples that follow can be characterized by Aspect ratio, Prandtl, Rayleigh and Stefan numbers, defined as

$$\mathrm{A} = \mathrm{W}/\mathrm{H} \tag{32}$$

$$\mathrm{Pr} = \frac{\mu c_p}{\lambda} \tag{33}$$

$$\mathrm{Ra} = \frac{g\beta\Delta T L^3 \rho^2 c_p}{\lambda\mu} \tag{34}$$

$$\mathrm{Ste} = \frac{\Delta T cp}{L} \tag{35}$$

where ΔT stands for the temperature difference, and W and H for cavity width and height. In order to consistently observe the time evolution of the system, dimensionless Fourier time is used on all figures where the time transients are presented

$$\mathrm{Fo} = \frac{\lambda}{\rho c_p \mathrm{H}^2} t \tag{36}$$

Dimensionless spatial coordinates, velocities and temperature are introduced as well

$$\begin{aligned} x &= \frac{p_x}{W}, \quad y = \frac{p_y}{W} \\ v_x &= \frac{\bar{v}_x W \rho c_p}{\lambda}, \quad v_y = \frac{\bar{v}_y W \rho c_p}{\lambda} \\ \Phi &= \frac{T - T_{COLD}}{T_{HOT} - T_{COLD}} \end{aligned} \tag{37}$$

where p_x, p_y, T, $\bar{v}_x$ and $\bar{v}_y$ stand for dimensional spatial coordinates, temperature and velocity components used in section Governing equations.(1) The Nusselt number is defined as

$$\mathrm{Nu}(x,y) = -\frac{\partial T(x,y)}{\partial x} + v_x(x,y)T(x,y) \tag{38}$$

The Nusselt number is calculated locally on a support of five collocation nodes, similar like other derivatives in the present work.

4.1 Natural convection in a tall cavity

A differentially heated closed cavity with A = 1/4, filled with Al-4.5%Cu like melt has been taken as a first benchmark problem. The initial temperature and velocity are set to zero. No phase change is assumed in this test case. The problem is additionally characterized by dimensionless numbers $\mathrm{Pr} = 0.0137$ and $\mathrm{Ra} = 2.81 \cdot 10^5$. The case is especially interesting due to its oscillating "steady-state"' which is a result of a balance between the buoyancy and the shear forces (Figure 5). This case is also relevant for fluid flow behavior in initial stages of melting of metals, since it has a similar geometrical arrangement (compare Figure 5 and Figure 19). This test case has been already computed by two different numerical methods [Založnik, Xin and Šarler (2005)] (spectral FEM and FVM) with good mutual agreement. Respectively, these solutions can be used for assessment of the present LRBFCM as well. The agreement between the present method and the other two numerical methods is excellent (Figure 4) despite entirely different space and time discretizations employed. The agreement of the system dynamics between the three methods used infers a high level of confidence in the present novel meshless method.

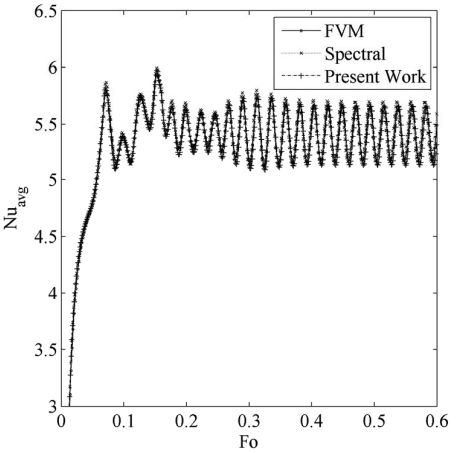

Figure 3: Hot-side average Nusselt number time development comparison: entire transient

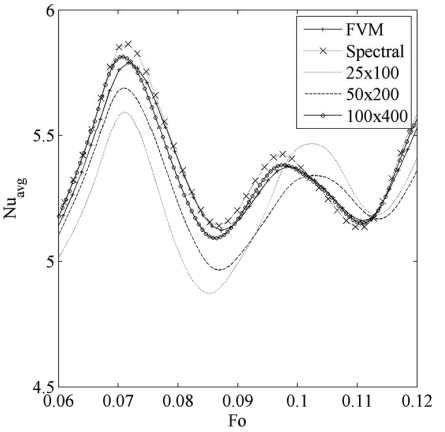

Figure 4: Hot-side average Nusselt number time development comparison: early stage detail

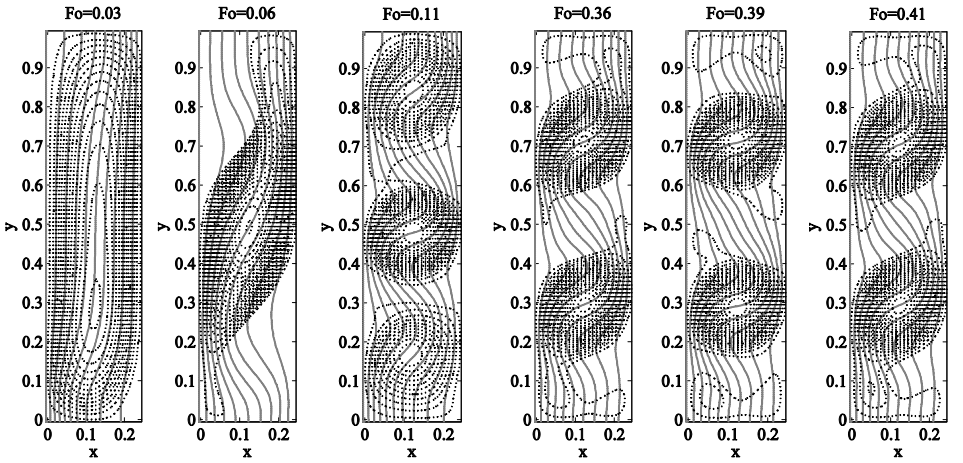

Figure 5: The early stage time development (first three figures) and "steady-state" oscillations (last three figures) of a tall cavity natural convection. Temperature contours are plotted as solid lines with contour step 0.1 and streamlines are plotted as dotted lines with a contour step 0.2

4.2 Melting benchmark test

The melting driven by natural convection, with differentially heated vertical walls and adiabatic horizontal walls, is solved next. The initial temperature is set to the $T_m + T_L$ and the whole domain is initially in the solid phase. The north and the south walls are insulated (Neumann boundary condition), the west wall is set to the temperature above the melting temperature and the east wall is set to the $T_m + T_L$. This test was first proposed by Le Quéré and Gobin [Gobin and Le Quéré (2000)]. Four different cases are calculated, two with low Prandtl and Stefan numbers and two with high Prandtl and Stefan numbers:

Table 1: Definition of melting cases

	Pr	**Ste**	**Ra**
Case 1	0.02	0.01	2.5e4
Case 2	0.02	0.01	2.5e5
Case 3	50	0.1	1.0e7
Case 4	50	0.1	1.0e8

The results are represented in terms of liquid-solid interphase boundary position, average hot-side Nusselt number time development, average liquid fraction time

development (Figures 6-Figure 19). Our results of the interphase boundary position are superimposed on the resuls of several other authors [Bertrand, Binet, Combeau, Couturier, Delannoy, Gobin, Lacroix, Quéré, Médale, Mencinger, Sadat and Vieira (1998)] (Figures 6-9) that participated in the Gobin Le Quéré benchmark test. The calculated interphase boundary position is within the dispersion of the results of other authors in all cases. The convergence of our method is checked on the melting Case 1. Several node distribution densities have been tested. It is evident from the Figure 11 that discretization under 21x21 nodes gives unreasonable results. From plots with finer discretizations (melting front - Figure 10 and temperature cross-sections at x=0.2 - Figure 11) 51x51, 101x101, 151x151 and 201x201, the convergence of the method is demonstrated. Both, melting front positions and temperature cross-sections, behave convergent. Additional convergence study has been done, where the mean temperature, and the mean melting front position are plotted with respect to the node distribution density (Figure 18).

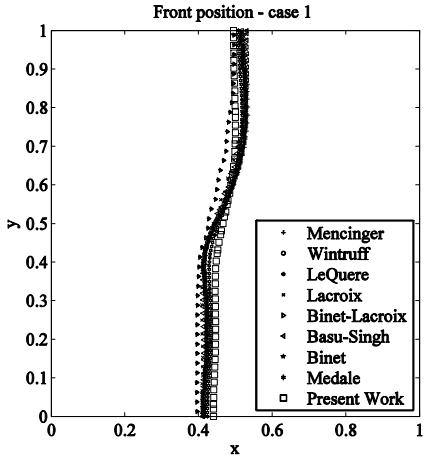

Figure 6: The melting front position at Fo=10, Case 1

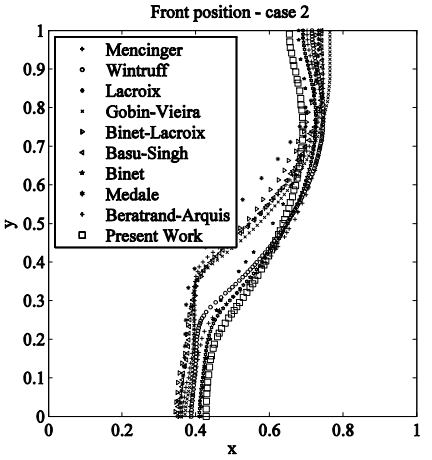

Figure 7: The melting front position at Fo=10, Case 2

4.3 Numerical parameters

The shape parameter C=30 and the five nodded overlapping sub-domain strategy has been used in all calculations. The pressure-velocity relaxation parameter is set to the same numerical value as time step for all cases and the characteristic length is set to the cavity width, other numerical parameters are stated in Table 3.

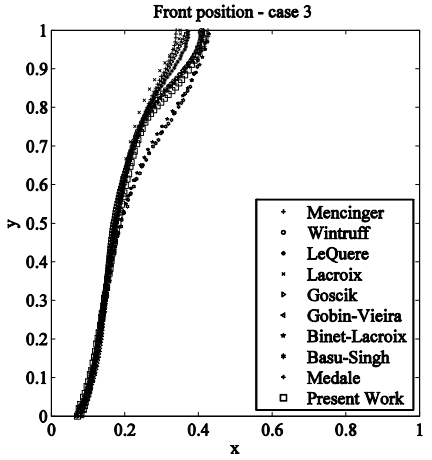

Figure 8: The melting front position for at Fo=0.1, Case 3

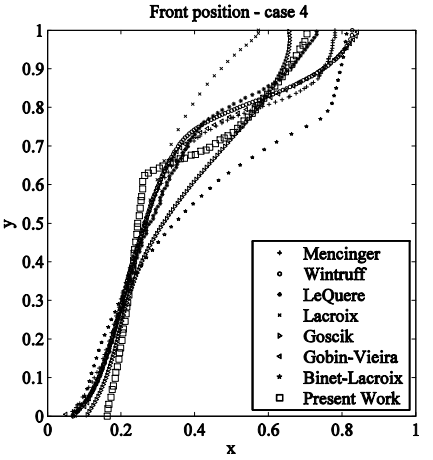

Figure 9: The melting front position at Fo=0.1, Case 4

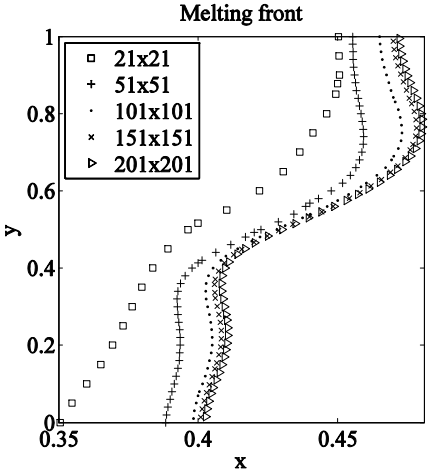

Figure 10: Discretization influence on the melting front position at Fo=10, Case 1

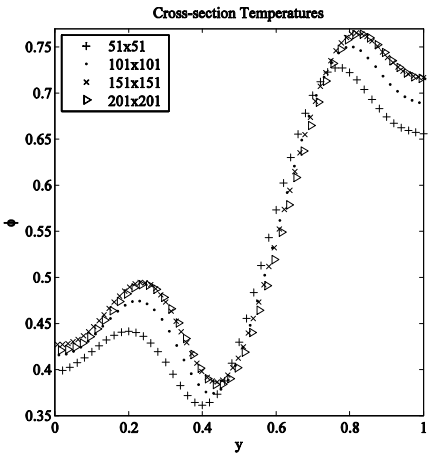

Figure 11: Discretization influence on the cross-section temperatures (x=0.2) at Fo=10, Case 1

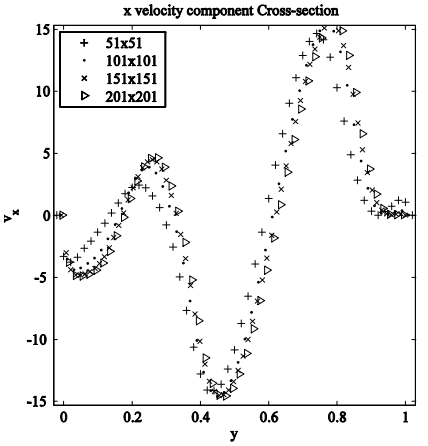

Figure 12: Discretization influence on the cross-section of x velocity component (x=0.2) at time Fo=10, Case 1

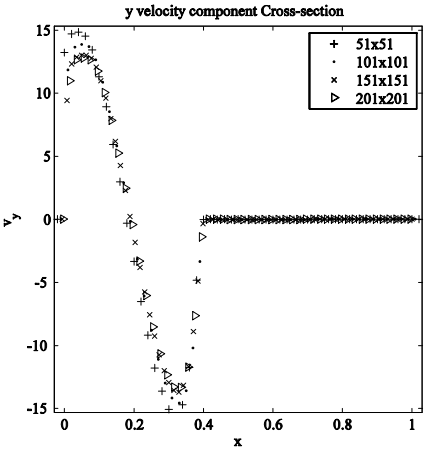

Figure 13: Discretization influence on the cross-section of y velocity component (y=0.5) at Fo=10, Case 1

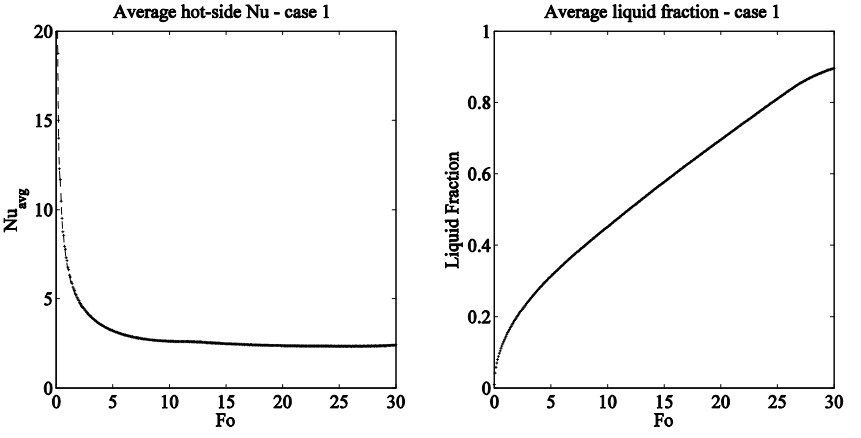

Figure 14: Hot-side average Nusselt number and average liquid fraction development as a function of Fo, Case 1

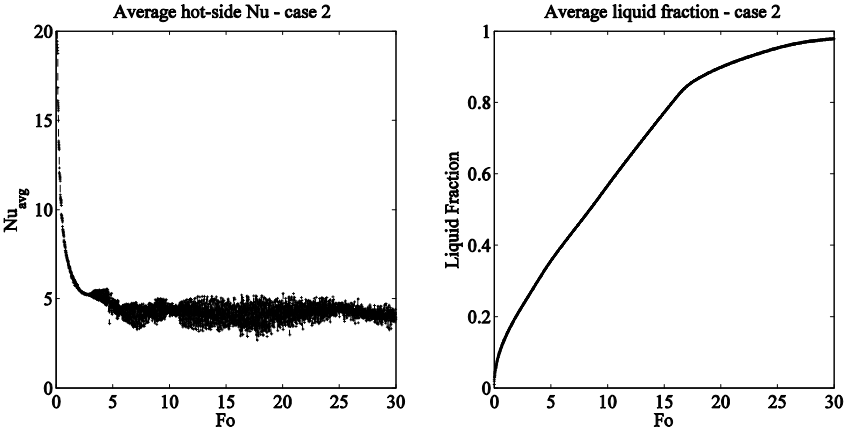

Figure 15: Hot-side average Nusselt number and average liquid fraction development as a function of Fo, Case 2

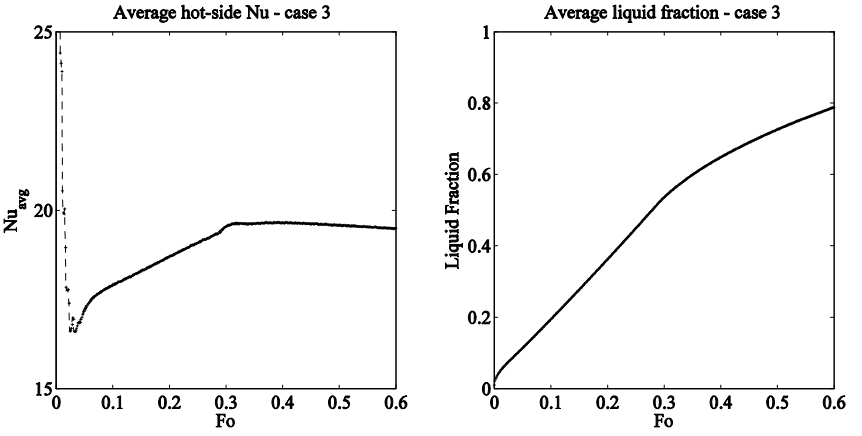

Figure 16: Hot-side average Nusselt number and average liquid fraction development as a function of Fo, Case 3

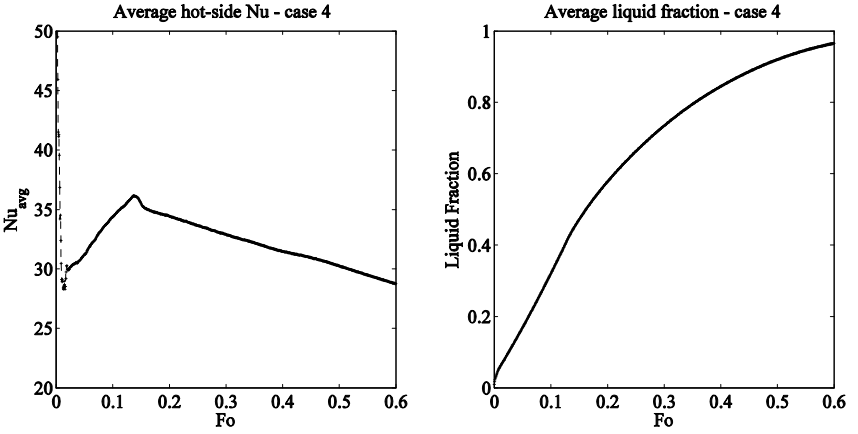

Figure 17: Hot-side average Nusselt number and average liquid fraction time development, Case 4

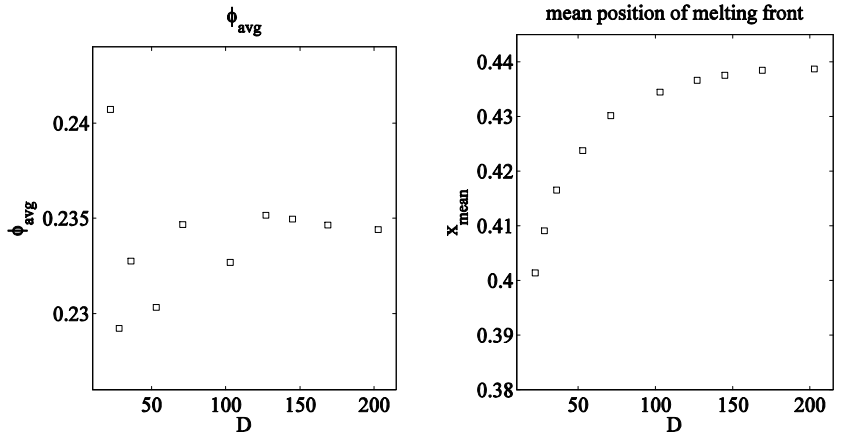

Figure 18: Average temperature (left) and mean melting front position (right) with respect to the discretization, Case 1

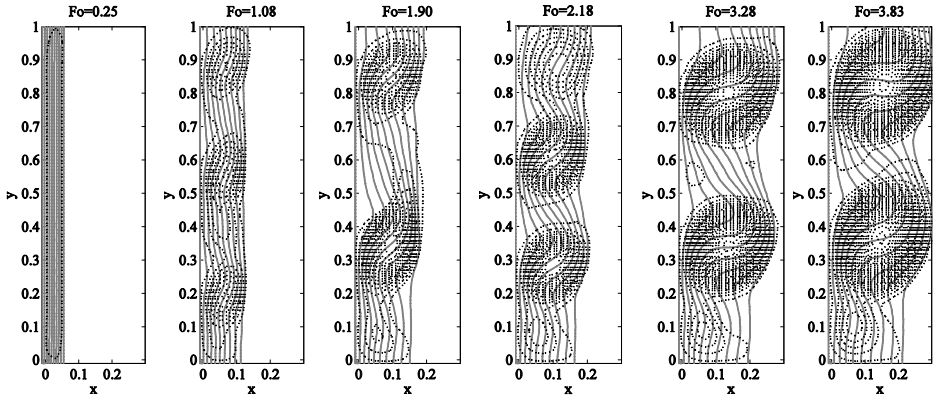

Figure 19: The early stage time development of temperature contours (solid line, step 0.1) and streamlines (dotted line, step 0.2), Case 2

Table 2: Interphase boundary positions (x,y) at Fo=10 for cases 1 and 2 and at Fo=0.1 for cases 3 and 4

y	Case 1	Case 2	Case 3	Case 4
0.0	0.4398	0.4270	0.0646	0.1568
0.1	0.4425	0.4339	0.0991	0.1793
0.2	0.4454	0.4583	0.1213	0.1983
0.3	0.4446	0.5272	0.1381	0.2146
0.4	0.4476	0.5926	0.1558	0.2283
0.5	0.4662	0.6403	0.1743	0.2403
0.6	0.4880	0.6743	0.1961	0.2534
0.7	0.4994	0.6919	0.2244	0.4390
0.8	0.4999	0.6919	0.2744	0.5662
0.9	0.4968	0.6755	0.366	0.6497
1.0	0.4955	0.6577	0.4156	0.7096

4.4 Mass conservation

Additional test is represented in order to evaluate the performance of the pressure-velocity coupling. The error of the pressure-velocity coupling algorithm propagates through the artificial mass loss due to the deviation from the divergence free velocity. The numerical mass leakage is computed as [Kosec and Šarler (2008a)]

$$\eta = -\Delta \mathrm{Fo} \sum_{j=0}^{J} \frac{1}{N} \sum_{i=1}^{N} \nabla \cdot \mathbf{v}_i(j\Delta \mathrm{Fo}) \tag{39}$$

Table 3: Numerical parameters

benchmark	**discretization**	**Fo time step (ΔFo)**	T_L/T_M	ε_V
Tall cavity	25x100	5.0e-6	n.a.	0.10
Tall cavity	50x200	2.5e-6	n.a.	0.10
Tall cavity	100x400	5.0e-7	n.a.	0.10
Case 1	51x51	1.0e-5	0.01	0.10
Case 1	101x101	1.0e-5	0.01	0.10
Case 1	151x151	1.0e-5	0.01	0.10
Case 1	201x201	5.0e-6	0.01	0.10
Case 2	101x101	5.0e-6	0.05	1.00
Case 3	101x101	1.0e-4	0.01	0.01
Case 4	101x101	1.0e-5	0.05	1.00

where N stands for the number of the nodes and $J = \mathrm{Fo}/\Delta\mathrm{Fo}$ for the number of the time steps. The results of the mass conservation are given in Table 4.

Table 4: Mass violation time integration

benchmark	Fo	η
Tall Cavity	0.25	1.74e-6
Case 1	10	8.02e-6
Case 2	10	2.58e-5
Case 3	0.1	1.31e-8
Case 4	0.1	1.92e-7

4.5 Discussion

The oscillations of flow structure and Nusselt number in the Case 2 were already reported by Mencinger [Mencinger (2003)]. A detailed discussion on the parameter range with appearance of the flow physics based oscillations can be found in the work [Hannoun, Alexiades and Zee Mai (2003)]. The behavior of the results of other three cases is in good agreement with the already known solutions [Gobin and Le Quéré (2000)]. There is a bit higher deviance in the Case 4, still the deviation of other authors for that case is very high and it is difficult to conclude which solution is more close to the correct solution at the present. The results of natural convection in a tall cavity are in exceptionally good agreement with the reference simulations.

5 Conclusions

The use of the LRBFCM in the thermo-fluid problems with phase change has been explored in the present paper. The completely local pressure-velocity coupling makes the algorithm entirely local. The straightforward implementation of the algorithm is simple and easy to upgrade to more complex physical and/or geometrical situations. The represented results agree with other authors within the expected dispersion. The agreement of the results and the excellent performance in the additional test with the high cavity low-Pr fluid encourages us to believe that the algorithm is suitable and reliable for solving the thermo-fluids with included phase change problems. Our future work will be focused on implementing the automatic local grid refinement with shape parameter optimization algorithm [Perko and Šarler (2007), Bourantas, Skouras and Nikiforidis (2009)] and inclusion of more complex physics (species transport and phase change of alloys).

Acknowledgement: The authors would like to express their gratitude to Slovenian Research Agency for support in the framework of the projects Young Researcher Programme 1000-06-310232 (G.K.), and Multiscale Modelling of Liquid-Solid Systems, J2-0099 (B.Š.).

References

Alexiades, V.; Solomon, A. D. (1993): *Mathematical Modeling of Melting and Freezing Processes*, Hemisphere Publishing Corporation, Washington, DC.

Atluri, S .N.; Shen, S. (2002a): *The Meshless Method*, Tech Science Press, Encino.

Atluri, S. N.; Shen, S. (2002b): The meshless local Petrov-Galerkin (MLPG) method: a simple & less-costly alternative to the finite element and boundary element methods. *CMES: Computer Modelling in Engineering & Sciences*, vol. 3, pp. 11-52.

Atluri, S.N. (2004): *The Meshless Method (MLPG) for Domain and BIE Discretization*, Tech Science Press, Forsyth.

Bertrand, O.; Binet, B.; Combeau, H.; Couturier, S.; Delannoy, Y.; Gobin, D.; Lacroix, M.; Quéré, P. Le; Médale, M.; Mencinger, J.; Sadat, H.; Vieira, G. (1998): Melting driven by natural convection. *Int. J. Therm. Sci.*, vol. 38, pp. 5-26.

Bourantas, GC; Skouras, ED; Nikiforidis, GC (2009): Adaptive Support Domain Implementation on the Moving Least Squares Approximation for Mfree Methods Applied on Elliptic and Parabolic PDE Problems Using Strong-Form Description *CMES: Computer Modeling in Engineering and Sciences*, vol. 43, pp. 1-25.

Buhmann, M.D. (2000): *Radial Basis Functions*, Cambridge University Press,

Cambridge.

Chen, C. S.; Ganesh, M.; Golberg, M. A.; Cheng, A. H. D. (2002): Multilevel compact radial basis functions based computational scheme for some elliptic problems. *Computers and Mathemathics with Applications*, vol. 43, pp. 359-378.

Chen, W. (2002): New RBF collocation schemes and kernel RBFs with applications. *Lecture Notes in Computational Science and Engineering*, vol. 26, pp. 75-86.

Crank, J. (1999): *Free and Moving Boundary Problems*, Oxford University Press, Oxford.

Dalhuijsen, A.J.; Segal, A. (1986): A comparison of finite element techniques for solidification problems. *Int.J.Numer Methods Eng*, vol. 23, pp. 1829-1986.

Dantzig, J.; Rappaz, M. (2009): *Solidification*, EPFL Press, Laussane.

Dantzig, J.A. (1989): Liquid-solid phase changes with melt convection. *International Journal of Numerical Methods in Engineering,*, vol. 28, pp. 1769-1785.

Divo, E.; Kassab, A. J. (2007): Localized meshless modeling of natural-convective viscous flows. *Numerical Heat Transfer, Part B*, vol. 129, pp. 486-509.

Fukusako, S.; Yamada (1993): Recent advances in research on water freezing and ice-melting problems. *Experimental Thermal Fluid Sciences*, vol. 6, pp. 90-105.

Gobin, D. ; Le Quéré, P. (2000): Melting from an isothermal verical wall, synthesis of a numerical comparison excercise. *Comp. Assist. Mech. Eng. Sc.*, vol. 198 pp. 289-306.

Hannoun, N. ; Alexiades, V. ; Zee Mai, T. (2003): Resolving the controversy over tin and gallium melting in a rectangular cavity heated from the side. *Numerical Heat Transfer, Part B*, vol. 44, pp. 253-276.

Haq, S.; ul-Islam, S.; Arshed, A. (2008): A numerical meshfree technique for the solution of the MEW equation. *CMES: Computer Modeling in Engineering & Sciences*, vol. 38, pp. 1-24.

Jany, P.; Bejan, A. (1987): Scaling theory of melting with natural convection in an enclosure. *International Journal of Heat and Mass Transfer*, vol. 31, pp. 1221-1235.

Kansa, E. J. (1990a): Multiquadrics – a scattered data approximation scheme with application to computational fluid dynamics, part I. *Computers and Mathematics with Applications*, vol. 19, pp. 127-145.

Kansa, E. J. (1990b): Multiquadrics – a scattered data approximation scheme with application to computational fluid dynamics, part II. *Computers and Mathematics with Applications*, vol. 19, pp. 147-161.

Kosec, G. ; Šarler, B. (2008a): Solution of Thermo-Fluid Problems by Collocation with Local Pressure Correction. *International Journal of Numerical Methods for Heat and Fluid Flow*, vol. 18, pp. 868-882.

Kosec, G.; Šarler, B. (2008b): Local RBF collocation method for Darcy flow. *CMES: Computer Modeling in Engineering and Sciences*, vol. 25, pp. 197-208.

Kovačević, I.; Poredoš, A.; Šarler, B. (2003): Solving the Stefan problem with the radial basis function collocation method. *Numer. heat transf. B Fundam.* , vol. 44, pp. 1-24.

Le, P.; Mai-Duy, N; Tran-Cong, T.; Baker, G. (2008): A meshless modeling of dynamic strain localization in quasi-brittle materials using radial basic function networks. *CMES: Computer Modeling in Engineering & Sciences*, vol. 25, pp. 43-66.

Le Quéré, P. ; Gobin, D. (1999): A note on possible flow instabilities in melting from the side. *Int. J. Therm. Sci.*, vol. 38, pp. 595-600.

Lee, C.K.; Liu, X.; Fan, S.C. (2003): Local muliquadric approximation for solving boundary value problems. *Computational Mechanics*, vol. 30, pp. 395-409.

Libre, N.A.; Emdadi, A.; Kansa, E.J.; Rahimian, M.; Shekarchi, M. (2008): A stabilised RBF collocation scheme for Neumann type boundary conditions. *CMES: Computer Modeling in Engineering & Sciences*, vol. 24, pp. 61–80.

Liu, G.R. (2003): *Mesh Free Methods*, CRC Press, Boca Raton.

Liu, G.R.; Gu, Y.T. (2005): *An Introduction to Meshfree Methods and Their Programming*, Springer, Dordrecht.

Mai-Cao, L.; Tran-Cong, T. (2005): A meshless IRBFN-based method for transient problems. *CMES: Computer Modeling in Engineering & Sciences*, vol. 7, pp. 149-171.

Mai-Cao, L.; Tran-Cong, T. (2008): A meshless approach to capturing moving interfaces in passive transport problems. *CMES: Computer Modeling in Engineering & Sciences*, vol. 31, pp. 157-188.

Mai-Duy, N.; Khennane, A.; Tran-Cong, and T. (2007): Computation of Laminated Composite Plates using Integrated Radial Basis Function Networks *CMC: Computers, Materials & Continua*, vol. 5, pp. 63-78.

Mai-Duy, N.; Mai-Cao, L.; Tran-Cong, T. (2007): Computation of transient viscous flows using indirect radial basic function networks. *CMES: Computer Modeling in Engineering & Sciences*, vol. 18, pp. 59-77.

Mai-Duy, N.; Tran-Cong, T. (2002): Mesh-free radial basis function network methods with domain decomposition for approximation of functions and numerical solution of Poisson's equations. *Engineering Analysis with Boundary Elements*,

vol. 26, pp. 133-156.

Mai-Duy, N.; Tran-Cong, T. (2003): Indirect RBFN method with thin plate splines for numerical solution of differential equations. *CMES: Computer Modeling in Engineering & Sciences*, vol. 4, pp. 85-102.

Mencinger, J. (2003): Numerical simulation of melting in two-dimensional cavity using adaptive grid. *Journal of Computational Physics*, vol. 198, pp. 243-264.

Perko, J.; Šarler, B. (2007): Weigh function shape parameter optimization in meshless methods for non-uniform grids. *CMES: Computer Modeling in Engineering and Sciences*, vol. 19, pp. 55-68.

Prescott, P.J; Incropera, F.P. (1996): Convection heat and mass transfer in alloy solidification. *Advances in Heat Transfer*, vol. 28, pp. 231-338.

Rettenmayr, M. (2009): Melting and Remelting Phenomena. *International Materials Reviews*, vol. 54, pp. 1-17.

Stella, F.; Giangi, M. (2000): Melting of a pure metal on a vertical wall: numerical simulation. *Numerical Heat Transfer, Part A*, vol. 38, pp. 193-208.

Stevens, D.; Power, H.; Lees, M.; Morvan, H. (2009): The use of pde data-centres on the local hermition interpolation meshless method for the numerical solution of convective-diffusion problems. *Journal of Computational Physics*, vol. 228, pp. 4606-4624.

Šarler, B. (1995): Stefan's work on solid-liquid phase changes. *Engineering Analysis with Boundary Elements*, vol. 16, pp. 83-92.

Šarler, B. (2002): Towards a mesh-free computation of transport phenomena. *Engineering Analysis with Boundary Elements*, vol. 26, pp. 731-738.

Šarler, B. (2005): A radial basis function collocation approach in computational fluid dynamics. *CMES: Computer Modelling in Engineering & Sciences*, vol. 7, pp. 185-193.

Šarler, B. (2007): From global to local radial basis function collocation method for transport phenomena. *Advances in Meshfree Techniques*, Springer, Berlin, pp. 257-282.

Šarler, B.; Gobin, D.; Goyeau, B.; Perko, J.; Power, H. (2000): Natural convection in porous media - dual reciprocity boundary element method solution of the Darcy model. *International Journal of Numerical Methods in Fluids*, vol. 33, pp. 279-312.

Šarler, B.; Kuhn, G. (1998a): Dual reciprocity boundary element method for convective-diffusive solid-liquid phase change problems, Part 1: Formulation. *Engineering Analysis with Boundary Elements*, vol. 21, pp. 53-63.

Šarler, B.; Kuhn, G. (1998b): Dual reciprocity boundary element method for convective-diffusive solid-liquid phase change problems, Part 2: Numerical Examples. *Engineering Analysis with Boundary Elements*, vol. 21, pp. 65-79.

Šarler, B.; Kuhn, G. (1999): Primitive variable dual reciprocity boundary element method solution of incompressible Navier-Stokes equations. *Engineering Analysis with Boundary Elements*, vol. 23, pp. 443-455.

Šarler, B.; Perko, J.; Chen, C. S.; Kuhn, G. (2001): A meshless approach to natural convection, *International Conference on Computational Engineering and Sciences, CD proceedings.*

Šarler, B.; Perko, J.; Chen, C.S. (2004): Radial basis function collocation method solution of natural convection in porous Media. *International Journal of Numerical Methods for Heat & Fluid Flow*, vol. 14, pp. 187-212.

Šarler, B.; Perko, J.; Gobin, D.; Goyeau, B.; Power, H. (2004): Dual reciprocity boundary element method solution of natural convection in Darcy–Brinkman porous media. *Engineering Analysis with Boundary Elements*, vol. 28, pp. 23–41.

Šarler, B.; Vertnik, R. (2006): Meshfree explicit local radial basis function collocation method for diffusion problems. *Computers and Mathematics with Applications*, vol. 51, pp. 1269-1282.

Vertnik, R; Šarler, B. (2009): Solution of incompressible turbulent flow by a mesh-free method. *CMES: Computer Modeling in Engineering and Sciences*, vol. 44, pp. 65-95.

Vertnik, R.; Šarler, B. (2006): Meshless local radial basis function collocation method for convective-diffusive solid-liquid phase change problems. *International Journal of Numerical Methods for Heat and Fluid Flow*, vol. 16, pp. 617-640.

Vertnik, R.; Založnik, M.; Šarler, B. (2006): Solution of transient direct-chill aluminium billet casting problem with simultaneous material and Interphase moving boundaries by a meshless method. *Engineering Analysis with Boundary Elements*, vol. 30, pp. 847-855.

Viskanta, R. (1988): Heat Transfer During Melting and Solidification of Metals. *Journal of Heat Transfer*, vol. 110, pp. 1205-1219.

Viswanath, R.; Jaluria, R. (1993): A comparison of different solution methodologies for melting and solidification problems in enclosures. *Num. Heat Transfer B*, vol. 24, pp. 77-105.

Voller, V. R.; Mouchmnov, A.; Cross, M. (2002): An explicit scheme for coupling temperature and concentration fields in solidification models. *Applied Mathemathical Modeling*, vol. 28, pp. 79-94.

Yao, L. S.; Prusa, J. (1989): Melting and freezing. *Advances in Heat Transfer*,

vol. 19, pp. 1-95.

Založnik, M.; Xin, S.; Šarler, B. (2005): Verification of a numerical model of macrosegregation in direct chill casting. *International Journal of Numerical Methods for Heat & Fluid Flow*, vol. 18, pp. 308-324.

Zerroukat, M.; Power, H.; Chen, C.S. (1998): A numerical method for heat transfer problems using collocation and radial basis functions. *Internation Journal of Numerical Methods in Engineering*, vol. 42, pp. 1263-1278.